Open Archive TOULOUSE Archive Ouverte (OATAO)

OATAO is an open access repository that collects the work of Toulouse researchers and makes it freely available over the web where possible.

Insight into the transport mechanism of solute removed in dialysis by a membrane with double functionality

D. Snisarenko[a], D. Pavlenko[b], D. Stamatialis[b], P. Aimar[a], C. Causserand[a,*], P. Bacchin[a]

[a] *Laboratoire de Génie Chimique, Université de Toulouse, CNRS, INPT, UPS, Toulouse, France*
[b] *Bioartificial Organs, Department of Biomaterials Science and Technology, MIRA Institute, Faculty of Science and Technology, University of Twente, 7500 AE Enschede, The Netherlands*

A B S T R A C T

The present study aims at shedding light on the transport mechanisms involved in a functionalized membrane designed for improving hemodialysis. This membrane is prepared by embedding absorptive micro particles within its porous structure. To understand the transport mechanism through the membrane and make suggestions for its optimization, a mathematical model coupling convection, diffusion and adsorption is developed and validated by comparison of experimental and theoretical results. In fact, the model provides a description of the concentration profile from the donor (feed) compartment across the several layers with different properties to the acceptor (dialysate) compartment. In addition, the model allows to predict the influence of various parameters such as molecule diffusivity, membrane thickness, presence of convection, content of adsorptive particles on the flux intensification across the membrane. Comparison with experimental measurements demonstrates that the model is able to describe the transmembrane mass flux variation over time as a function of hydrodynamic conditions and membrane/module geometric parameters. The model also illustrates how the proposed double-layer membrane concept offers significant benefits in terms of toxin removal in comparison to conventional dialysis. As so, the main achievement of the developed model is that it may serve as tool for the further improvement of functionalized membrane in terms of toxin removal and optimization of process conditions.

Keywords:
Hemodialysis
Mathematical model
Double-layer membrane
Blood toxins removal

1. Introduction

Hemodialysis is a life-sustaining treatment that patients undergo when their kidneys malfunction. Even though this technique is constantly being improved for more than four decades it is still one of the major healthcare problems with high mortality and morbidity of the patients. High mortality rates are usually attributed to incomplete removal of the blood toxins during the dialysis treatment (Dobre et al., 2013; Meyer et al., 2011; Vanholder et al., 2015). The treatment provides adequate removal of only the small water soluble molecules, such as urea or creatinine. However, larger solutes, referred to as middle molecules and the protein-bound toxins, have inadequate clearance even after the development of more permeable high-flux hemodialyzers (Eloot et al., 2012; Luo et al., 2009).

As this extracorporeal treatment is primary driven by diffusion, the use of high volumes of pure dialysate liquid is necessary to maximize the concentration gradients across the membrane (Walther et al., 2006). Large volumes of high-quality dialysate solution make such an approach not only expensive, but also challenging for countries with scarce water resources. Besides, it was demonstrated in various studies

---

a	Specific surface area of the adsorbent (m^2 per m^3 of mixed matrix membrane)
c	Concentration ($mol\,m^{-3}$)
d	Diameter (m)
D	Diffusion coefficient ($m^2\,s^{-1}$)
div	Divergence (–)
j	Molar flux density ($mol\,m^{-2}\,s^{-1}$)
J	Convective flow through the membrane ($m\,s^{-1}$)
k	Heterogenic adsorption constant ($m\,s^{-1}$)
K	Pseudo mass transfer conductance ($m\,s^{-1}$)
l	Length of the fiber (m)
m	Mass (kg)
M	Molecular weight ($g\,mol^{-1}$)
N	Number of fibers (–)
Pe	Peclet number (–)
q	Quantity of adsorbed specie (μg per mg of membrane)
r	Rate of adsorption ($mol\,m^{-3}\,s^{-1}$)
Re	Reynolds number (–)
s	Sink term ($mol\,m^{-3}\,s^{-1}$)
S	Membrane surface area (m^2)
Sc	Schmidt number (–)
Sh	Sherwood number (–)
t	Time (s)
V	Volume of fluid (m^3)

Greek letters

δ	Thickness of the domain (m)
Δ	Determinant defined in Eq. (5) (–)
ϕ	Thiele modulus (–)

Subscripts

0	Initial time point
a	After the adsorptive layer
ads	Adsorption
b	Before the adsorptive layer
$conv$	Convection
d	Dialysate
$diff$	Diffusion
e	External
f	Feed
h	Hydraulic
in	At the inlet of particular domain
l	Lumen of the membrane
max	Maximal
out	At the outlet of particular domain
s	Shell side of the module
t	Time different from 0

(Barreto et al., 2009; Busch et al., 2010; Liabeuf et al., 2011; Raj et al., 2000) that poor removal of some uremic toxins (i.e. β-2-microglobulin), leads to other long-term hemodialysis related complications. Thus, there is an urgent need of new improvement of dialysis in order to overcome highlighted drawbacks.

A novel specific approach to maintain the beneficial high gradients across the dialysis membrane along with facilitated transport of uremic solutes was discussed by Meyer et al. (2007). There, addition of the sorbent to the dialysate solution resulted in significant increase of removal rates of various protein-bound toxins even without high dialysate flow rates. Such results demonstrated the great opportunities of combining the benefits of adsorption and filtration. More recently,

some of the authors of this work developed and proved the concept of the double layer mixed matrix membranes (Pavlenko et al., 2016; Tijink et al., 2013, 2012). These membranes consist of two layers: (1) a mixed matrix layer, where activated carbon particles are incorporated inside a porous polymer matrix; (2) a particle-free selective layer providing hemocompatibility and selectivity. Such design makes it possible to gain the benefits of the adsorption and diffusion in one step. In particular, membranes in both flat and hollow fiber double layer geometries showed an excellent removal of small and protein-bound toxins from human plasma giving high promise for their further development for dialytic applications.

However, the contribution of the mixed matrix layer to the removal of the uremic toxins, as well as the influence of the membrane characteristics and process conditions need to be quantified on an experimental and on a theoretical point of view. It is for example important to know how to optimize the transfer through a mixed matrix membrane. To tackle this question, in this work, we developed a model with various parameters and their physical relationships, in order to describe the overall performance of the membrane towards removal of small and middle-sized uremic toxins. The objective of this model is to offer an analytical and non-numerical problem resolution and to give the opportunity to optimize the membrane properties and process conditions. The upcoming sections are organized in the following manner: first, the selected assumptions along with mathematical derivation of required equations are described in order to formulate the model. Secondly, the fabrication and characterization of functionalized double-layer membranes is presented. Then, the prediction of solute concentration profiles across the membrane with use of the model is demonstrated. Finally, the developed model is validated by the comparison with the experimental results.

2.   Model development

A model is presented to describe the coupling of transport phenomena (advection, diffusion and adsorption) by describing the mixed matrix membranes by composite layers (Section 2.1). This one dimension model allows determining the concentration profile and the mass flux across the membrane and then the efficiency improvement due to the adsorbent (Section 2.2). In a last Section 2.3, this model for the transfer through the membrane is combined with the mass flux balances on the blood and dialysate side in order to depict the clearance variation along dialysis.

2.1.   Mass balance in the layers composing the mixed matrix membrane

The geometry of the system was dictated by the novel concept of blood filtration, which employs the membranes functionalized with adsorptive particles (Tijink et al., 2012). In its way through the membrane, a toxin present in the blood (feed stream) first passes through the particle-free layer (PFL) and then through the mixed matrix layer, where it can adsorb on the dispersed adsorptive particles as depicted in Fig. 1. The effect of the flow parallel to the membrane in the feed (blood) and dialysate side are modelled with boundary layers thickness. At the end, a four-layers system (Fig. 1) describe the mixed matrix membrane.

The model of solute transport through this system relies on following assumptions:

1) Superficial resistances are accounted through an averaged boundary layer thickness along the Y axis (Fig. 1);
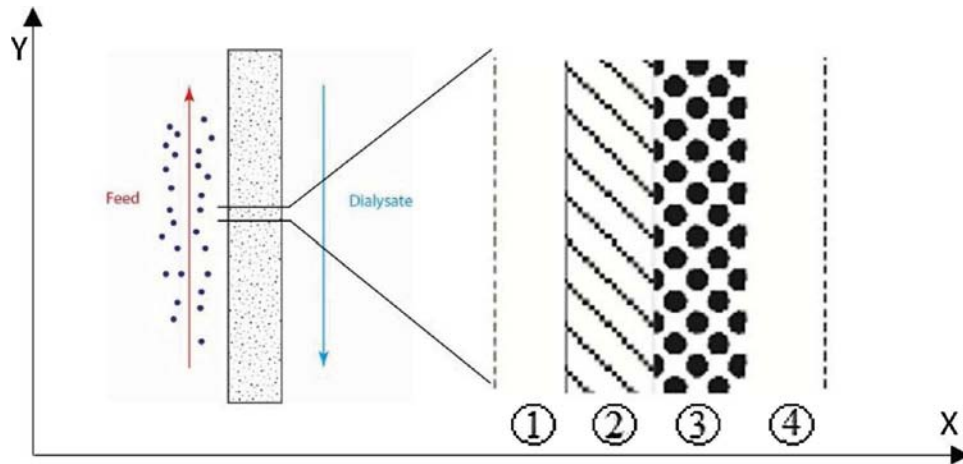2) Steady state for the transfer is considered through the membrane;

Fig. 1 – The schematic representation of the system geometry (dots in the feed represent the toxin molecules present in the blood stream). 1 — feed side boundary layer, 2 — particle-free membrane, 3 — mixed matrix membrane, 4 — dialysate boundary layer.

3) Cartesian coordinates are used to describe a planar membranes or hollow fibers when the boundary layer thickness are small compared to the fiber lumen;

4) Fluids in the blood and dialysate compartments are Newtonian;

5) Adsorptive particles are considered to be uniformly dispersed inside the polymeric matrix;

6) Adsorption is considered as first order heterogeneous reaction. Dealing with the adsorption mechanism, such a kinetic condition can correspond to the system where the adsorptive capacity is large compared to the amount to be adsorbed.

7) The transfer inside the adsorptive particles is not diffusion-limited. The particles are small enough to avoid a diffusion-controlled adsorption inside the particles.

8) The solute is considered small enough for its rejection by the membrane can be considered to be zero. Hence, the partition coefficient is then taken equal to one. In the case of future applications in which the solute would not be small compared to the pore size, the model could be easily modified to integrate a partition coefficient between the bulk and the membrane in order to take into account the effect of pore on the selectivity.

The mass transport of solute across the membrane is conventionally described by the generic continuity equation in the form of Eq. (1):

$$\frac{\partial c}{\partial t} + div\,(j) = \pm s \tag{1}$$

where s is the sink term which represents here the adsorption of the permeating solute.

As the model is being developed for the steady state condition, the time derivative of the solute concentration is nil here. Besides, analyzing the geometry of the model one may distinguish two types of regions depending on the possible toxin removal mechanisms: ones with convection and diffusion only (parts 1, 2 and 4 in Fig. 1), and one layer where, in addition to these two mechanisms, adsorption also takes place (part 3 in Fig. 1). At steady state and for Cartesian coordinates, the total molar flux, j, in the region without adsorbent
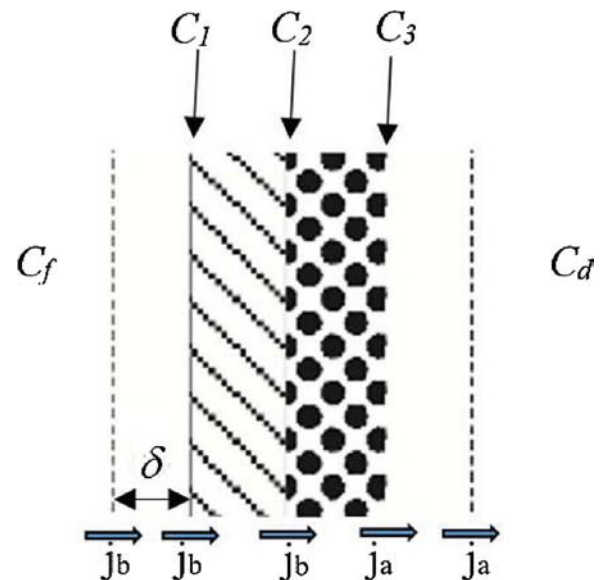

Fig. 2 – Schematic representation of formulated system with the key parameters for the different layers represented in Fig. 1.

($s = 0$) is constant (Eq. (1)) and has a diffusive and an advective contributions (Eq. (2)):

$$j = -D\frac{dc}{dx} + Jc \tag{2}$$

where c is the local solute concentration gradient, x is the distance along the direction normal to the membrane surface, D is diffusion coefficient, and J is convective flow through the membrane.

If assuming a given concentration at the inlet and the outlet, the integration of Eq. (2) gives the mass flux across the regions of the system without adsorptive particles.

$$j = J\frac{\left(c_2 - c_1 e^{\frac{J\delta}{D}}\right)}{1 - e^{\frac{J\delta}{D}}} \tag{3}$$

where c_2 and c_1 stand for the concentrations at the outlet and the inlet of the particular region of thickness δ (Fig. 2).

The application of Eq. (1) to the MMM layer results in a differential equation (Eq. (4)), which apart from diffusive and convective terms, also accounts for the presence of solute adsorption:

$$D\frac{d^2c}{dx^2} - J\frac{dc}{dx} - akc = 0 \qquad (4)$$

where a stands for specific surface area of adsorbent in m^2 per m^3 of mixed matrix membrane and k is heterogenic adsorption constant. The Eq. (4) is integrated through the MMM layer by considering as boundary conditions fixed concentration, c_2 and c_3 at the inlet and the outlet of the layers respectively (Fig. 2). The details of the integration are presented in the Supplementary information 1. It results in Eq. (5), which describes the solute concentration at any depth (x) inside the MMM layer:

$$c = c_3 \frac{e^{\left(\frac{Pe_3}{2}\left(\frac{x}{\delta_3}-1\right)\right)}\sinh\left(\frac{x\Delta}{\delta_3}\right)}{\sinh(\Delta)} - c_2 \frac{e^{\frac{Pe_3}{2}\frac{x}{\delta_3}}\sinh\left(\Delta\left(\frac{x}{\delta_3}-1\right)\right)}{\sinh(\Delta)} \qquad (5)$$

where $\Delta = \frac{\sqrt{Pe_3^2+4\varphi^2}}{2}$; $Pe_3 = \frac{J\delta_3}{D_3}$; $\varphi = \sqrt{\frac{ak}{D_3}}\delta_3$. Pe_3 is the Peclet number (ratio of advection over diffusion) in the MMM layer (part 3 in Fig. 1) and φ is the Thiele modulus representing the ratio of the reaction on the diffusion rate inside the MMM layer.

The molar flux before the MMM layer (j_b), and after (j_a) are determined by writing the molar flux Eq. (2) at the inlet $x = 0$ and the outlet $x = \delta_3$ boundaries respectively:

$$j_b = c_2\left(\frac{D_3\Delta\cosh(\Delta)}{\delta_3\sinh(\Delta)} + \frac{D_3Pe_3}{2\delta_3}\right) - c_3\frac{D_3e^{-\frac{Pe_3}{2}}\Delta}{\delta_3\sinh(\Delta)} \qquad (6)$$

$$j_a = c_2\frac{D_3e^{\frac{Pe_3}{2}}\Delta}{\delta_3\sinh(\Delta)} - c_3\left(\frac{D_3\Delta\cosh(\Delta)}{\delta_3\sinh(\Delta)} - \frac{D_3Pe_3}{2\delta_3}\right) \qquad (7)$$

Finally, the solute molar flux density before this layer is greater than the one after, $j_b > j_a$; the difference being relative to the adsorption rate of the permeating species inside the MMM. Summarizing the aforementioned model formulation, the schematic description of the entire system with its key parameters (interface concentrations and fluxes) involved is presented in Fig. 2.

2.2. Global mass flux across the mixed matrix membrane

The model is established by considering the continuity of the molar flux before and after the MMM layer. The following system of five equations with two unknown molar flux densities j_b and j_a, and three unknown concentrations at the interfaces of domains c_1, c_2 and c_3 has to be solved:

$$\begin{cases} j_b = c_f K_{1a} - c_1 K_{1b}; \\ j_b = c_1 K_{2a} - c_2 K_{2b}; \\ j_b = c_2 K_{3a} - c_3 K_{3b}; \\ j_a = c_2 K_{3c} - c_3 K_{3d}; \\ j_a = c_3 K_{4a} - c_d K_{4b}; \end{cases} \qquad (8)$$

The expressions for each pseudo mass transfer conductance ($K_{i,j}$) are determined from the writing of the differential molar balances presented in the previous section. The expressions for these conductances are given in the Appendix A.

The solution for the concentration of the permeating species on the interfaces adjacent to the adsorptive layer c_2 and c_3 are given below:

$$c_2 = \frac{K_{1a}K_{2a}(K_{4a}+K_{3d})c_f + K_{3b}K_{4d}(K_{2a}+K_{1b})c_d}{(K_{3a}(K_{2a}+K_{1b})+K_{1b}K_{2b})(K_{4a}+K_{3d}) - K_{3b}(K_{2a}+K_{1b})K_{3c}} \qquad (9)$$

$$c_3 = \frac{K_{1a}K_{2a}K_{3c}c_f + (K_{3a}(K_{2a}+K_{1b})+K_{1b}K_{2b})K_{4d}c_d}{(K_{3a}(K_{2a}+K_{1b})+K_{1b}K_{2b})(K_{4a}+K_{3d}) - K_{3c}K_{3b}(K_{2a}+K_{1b})} \qquad (10)$$

Combining these last two expressions with Eq. (6) and Eq. (7), enables determining the molar flux uphill and downhill the MMM layer.

The properties of the layers (solute diffusion coefficients and thickness) and the operating conditions (rate of convective flow, adsorption constant and solute concentration on both sides of a membrane) provide the possibility to analyze the transfer through the system at a particular time of the dialysis process.

Furthermore, the model enables analyzing the impact of the adsorptive particles on the local solute concentration inside the MMM. The transfer efficiency can be compared with the pure diffusion case for different scenarios such as: (a) absence of convection (solute removal occurs only by diffusion and adsorption); (b) absence of adsorption (presence of diffusion and convection), and (c) absence of both convection and adsorption. The benefit of the functionalized membrane compared to a conventional single layer membrane of same thickness can be defined through a solute transport enhancement factor (STEF):

$$STEF = \frac{j_b}{j_{diff}} \qquad (11)$$

In practice, STEF is defined as a ratio of molar flux density (j_b) obtained in one of the aforementioned scenarios to the molar flux density obtained when only diffusive transport is involved (j_{diff}). The diffusive case is used as a reference of classical dialysis and thus STEF demonstrates the intensification of the solute removal due to the contribution of convection or/and adsorption.

In general, membrane fouling phenomena due to protein adhesion on the membrane, as well as, other phenomena such as blood coagulation and thrombus in the membrane module can also play a role on the solute transfer when working in real conditions with blood. Such phenomena would induce an additional superficial mass transfer resistance that could be accounted for in an improved version of the model. The MMM are specifically designed to minimise these phenomena. The particle free membrane layer which is in direct contact with blood, is made by PES/PVP polymer blend, also used in the development of the commercial dialysis membranes and has very good blood compatibility. In fact, our recent study showed that the MMM can achieve superior removal of protein bound toxins from human plasma compared to commercial dialysers without fouling phenomena (Pavlenko et al., 2016)

Table 1 – Spinning conditions of the fiber preparation.

	Membrane 1	Membrane 2
Inner layer pumping flow (mL/min)	0.4	0.9
Outer layer pumping flow (mL/min)	1.6	3.2
Bore pumping flow (mL/min)	2.8	2.7
Bore composition	Demi water	5 wt% PVP in ultra pure water
Air gap (cm)	10	–
Pulling speed (m/min)	3.5	7
Content of PVP in the dope solution for selective layer (wt%)	7	10

Table 2 – Spinneret specifications.

	Membrane 1	Membrane 2
Inner diameter needle (mm)	0.16	0.26
Outer diameter needle (mm)	0.26	0.46
Inner diameter first orifice (mm)	0.46	0.66
Outer diameter first orifice (mm)	0.66	0.96
Inner diameter second orifice (mm)	0.86	1.66

Table 3 – Uremic toxins.

Type	Specific properties	Main representatives
Unbound small	<500 Da	Urea, creatinine
Unbound middle	500 Da–60 kDa	Leptin, endothelin, β_2-microglobulin
Protein bound	Capable of protein binding	Indoxyl sulfate, p-cresol

Table 4 – Characteristics of β2-microglobulin and α-lactalbumin.

Protein	Molecular weight, kDa	pI
β_2-Microglobulin	11.8	5.7
α-Lactalbumin	14.2	4.5

2.3. Clearance and dialysis modelling

The model presented in the previous section helps to determine the mass flux for given conditions of concentration across the membrane. This mass flux defines the clearance for a given time of the dialysis. In order to depict the whole dialysis process, the mass flux (Eqs. (6), (8) and (10)) has to be solved together with mass balances on the feed compartment and on the dialysate compartment. The global (Eqs. (12) and (13)) and the partial mass balance (Eqs. (14) and (15)) for the feed and the dialysate side are:

$$\frac{dV_f}{dt} = -JS \quad (12)$$

$$\frac{dV_d}{dt} = JS \quad (13)$$

$$\frac{d\left(c_f V_f\right)}{dt} = -j_b S \quad (14)$$

$$\frac{d\left(c_d V_d\right)}{dt} = j_a S \quad (15)$$

where c_f and c_d stand for the solute concentration in the feed and dialysate, S is the filtration surface area, V_f and V_d are volumes of feed and dialysate.

If considering that the transient characteristic time for the mass flux establishment is very small compared to the order of magnitude of the dialysis time, the model can be solved for pseudo steady state conditions (considering a succession of steady state for the transfer). The integration of Eqs. (12)–(15) combined with the mass flux given in the previous section enables the determination of the variation of the solute concentration in the blood and the dialysate and then the clearance kinetics.

3. Validation experiments

3.1. Membrane fabrication and characterization

Double layer mixed matrix membranes were prepared according to a multistep procedure. For the selective layer, a polymer solution was prepared by dissolving 15% polyethersulfone (PES, Ultrason E 6020, BASF, Germany) and polyvinylpyrrolidone (PVP, K90, Fluka, Germany) of different quantity (details in Table 1) in ultra-pure N-methylpyrrolidone (NMP, Acros Organics, Belgium). Adsorptive layer was based on a solution containing 14% PES and 1.4% PVP dissolved in NMP. Activated carbon (AC) with average diameter of 27 μm was added gradually to the polymer solution to obtain a final concentration of 60% by weight. Both solutions were degassed for 48 h before the spinning.

Two different spinning conditions were utilized aiming to obtain membranes of different transport properties. The first batch of membranes (further denoted as Membrane 1) was formed via immersion precipitation method at the conditions summarized in Table 1. The second batch of membranes (hereon denoted as Membrane 2) was fabricated according to the procedure described by Tijink et al. (2013) with the conditions, which are also presented in Table 1.

Table 2 describes the specification of used spinnerets.

The membranes were cleaned by ultra-pure water to remove the remaining solvent. The fibers were then dried at 37 °C for 2 h and subsequently were fractured in liquid nitrogen. The samples were dried under vacuum at 30 °C and gold sputtered using a Balzers Union SCD 0 40 sputter coater (Oerlikon Balzers, Balzers, Liechtenstein). Finally, samples were imaged using a JEOL JSM-560 0LV Scanning Electron Microscope (JEOL, Tokyo, Japan).

Dry fibers were cut into pieces of 15 cm each and then glued into modules (inner diameter of 4 mm) of 3 fibers each, and 10 cm in length. Clean-water flux was then measured for each module with use of the set-up (Fig. 3 from Pavlenko et al., 2016) described in detail in the following section. For this, modules were initially pre-pressurized at 2 bar for 1 h and then tested at transmembrane pressures of 0.5, 1.0, 1.5 and 2.0 bar, with ultrapure water. The mass of collected permeate was monitored continuously.

3.2. Adsorption kinetics in static mode

At this stage, the knowledge of the adsorptive capacity of the carbon particles is an important issue. Experiments were conducted to determine the kinetics of adsorption of creatinine and α-lactalbumin onto the membrane. These two solutes have been chosen as models to illustrate the potentialities and the limitation of mixed matrix membranes in the removal of unbound small and middle uremic toxins (Table 3).
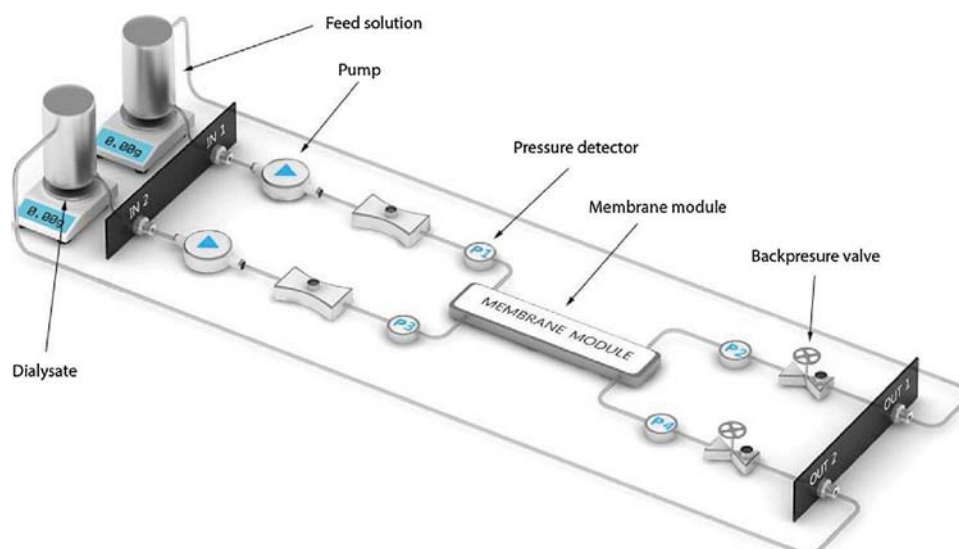
Fig. 3 – Schematic representation of the applied set-up (from Pavlenko et al., 2016).

Creatinine was selected as a model of unbound small toxins group when α-lactabumin was selected as a model compound for unbound middle-sized toxins such as β_2-microglobulin. Similarities between the molecular weight and the Isoelectric point of both proteins justify this choice (Table 4).

For the purpose of kinetics of adsorption study, five pieces of hollow-fiber membranes of 5 cm each were placed in 25 mL of 0.1 g/L solution of creatinine or α-lactalbumin in phosphate buffer solution (PBS). The solution was stirred to avoid transport limitations between solute and surface of adsorptive layer of the membrane. The decay of solute concentration with time was monitored by sampling of 0.5 mL/sample every 3 min for further analysis by UV-spectroscopy. The timing of sample collection was adjusted so as to limit the total withdrawal of initial volume at 10%. A linear decrease of the solute concentration in the initial stage of the process was observed. The initial slope of the concentration decrease provides an information on the rate of adsorption which may be used in the calculation of the product of the adsorption constant and specific surface area of adsorbent (ak).

3.3. Experimental study of the clearance of small and middle sized solutes

The experimental analysis of the clearance of solutes with the dual-layer membranes was conducted with use of the set-up (Convergence B.V., Enschede, The Netherlands) presented on Fig. 3.

Briefly, the experimental set-up consists of 2 peristaltic pumps, 4 pressure detectors, 2 back-pressure valves and 2 reservoirs for the model solutions (Pavlenko et al., 2016). All the parts of the set-up are connected via PTFE tubings to membrane module which has inlets and outlets for the feed and dialysate solutions that are pumped in counter-current configuration. The flow rates of the feed and dialysate solutions are controled by the peristaltic pumps, while constant TMP is generated by the back-pressure valves. Pressure in the system is monitored by 4 pressure detectors which are located near the membrane module's inlets and outlets. Compartments for the module solutions are positioned on the balances to control the mass of the system over time.

For the validation experiment, PBS-based 0.1 g/L solutions of creatinine (Sigma–Aldrich, France) as a model molecule for the small uremic toxin; and α-lactalbumin (Sigma–Aldrich, France) as a model compound for the middle-sized molecule were prepared, and were further used as feed solutions. The pure solution of PBS was used as the dialysate.

Validation experiments were conducted using 50 mL of the feed and dialysate solutions. Moreover, we followed the convention that the flow rate of the dialysate has to be twice as high as the flow rate of the feed stream (Henrich, 2009). As such, the feed flow rate was set as 5 mL/min, while the dialysate flow was equal to 10 mL/min. In addition, the feed solution was flown inside the hollow fiber membrane lumen, while the dialysate was pumped through the shell side of the module. For experiments in diffusive mode (conventional dialysis), the transmembrane pressure (TMP) was kept around 0 bar, meaning that the toxin removal driving force was generated only by the difference of its concentration across the membrane. In contrary, another set of experiments was conducted with utilization of both diffusion and convection (hemodiafiltration mode). There the TMP was set at 0.17 bar or 0.5 bar in different experiments in order to induce the convective transport through the membrane. These pressure regimes were chosen in order to, on one hand, avoid the necessity to add more feed to the system during the experiment, and on the other hand, to generate a convective flow with a noticeable impact on the overall solute removal. Throughout the experiment, the weight of the feed and dialysate solutions was continuously monitored. The decrease of the feed (increase of the dialysate) mass was considered to be due to the presence of convection. Samples of 1 mL were taken from both compartments at the same time and the concentration of creatinine and α-lactalbumin was measured by UV-spectroscopy (Varian, Cary 300 Scan UV–visible Spectrophotometer) at 25 °C in a 10 mm quartz cuvette at 230 nm and 280 nm, respectively. The increase in solute concentration in the dialysate was ascribed to the diffusive transport, in case of the experiment conducted in diffusive mode (conventional dialysis) or to a combination of diffusion and convection for experiments performed in hemodiafiltration mode. In parallel, based on mismatch between the amount of solute disappeared from the feed side and found in the dialysate the quantity of solute adsorbed
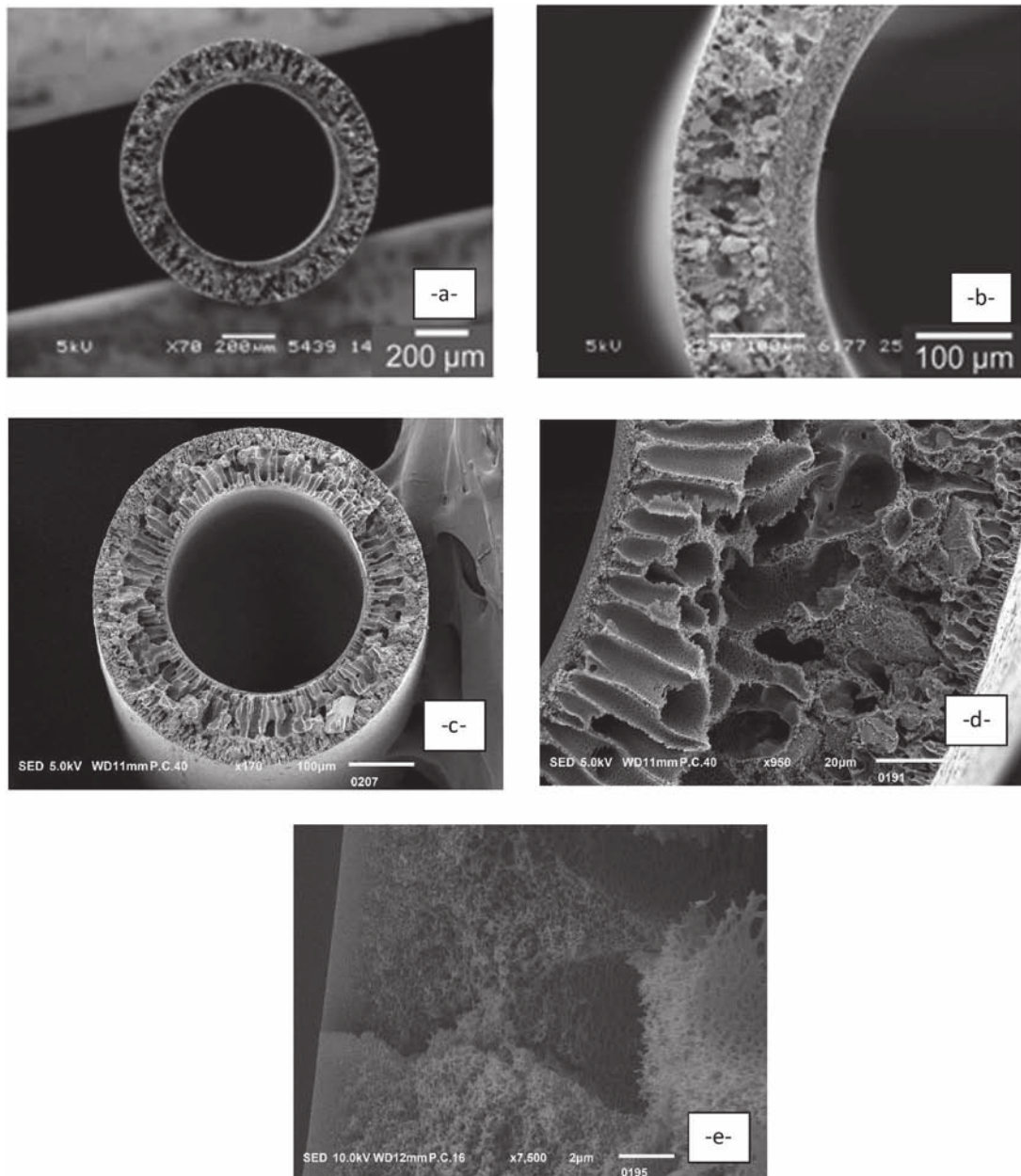
Fig. 4 – SEM images of the dual-layer MMM (Membrane 2: -a- and -b-; Membrane 1: -c-, -d- and -e-).

inside the membrane was defined. Finally, the total solute removal was considered to be the sum of diffusive/convective and adsorptive removals. Each validation experiment was conducted three times. After the experiments, the modules were dried in air and the effective surface area of membrane inside the module was measured.

4. Results and discussion

4.1. *Membrane fabrication and characterization*

Fig. 4 demonstrates the structure and the morphology of the membranes.

Fig. 4 compares the images of the Membrane 2 (Fig. 4 a,b) and Membrane 1 (Fig. 4 c–e) discussed in this study. For both membranes, one can distinguish the inner particle-free region with a denser skin layer on the lumen side and the outer particle-loaded (MMM) layer. In both cases, the two layers are well attached, the MMM layer is more porous and the particle-free inner selective layer, mainly determines to the

Table 5 – Geometrical dimensions of the fabricated fibers.		
	Membrane 1	Membrane 2
Thickness of the inner layer, μm	21	49
Thickness of MMM, μm	47	111
Lumen diameter, μm	450	669
External diameter of the fiber, μm	586	984

mass transport resistance of the entire membrane. For the Membrane 1, the particle free inner has a dense skin (see Fig. 4-e-) and a rather finger like pore morphology towards the MMM layer. For the Membrane 2, the inner particle free layer has overall sponge like morphology and is less dense (see Fig. 4-b-). For both membranes 1 and 2, SEM images suggest that the activated carbon particles are quite uniformly distributed inside the polymeric matrix. In general, Membrane 1 is much thinner than Membrane 2. The dimensions of the fibers are summarized in Table 5. These values were further

Table 6 – Values of reaction kinetic parameter, ak, for various systems "Membrane-solute".		
	Membrane 1	Membrane 2
Creatinine	$0.152\,s^{-1}$	$0.082\,s^{-1}$
α-Lactalbumin	–[a]	$0.011\,s^{-1}$

[a] Was not determined, because Membrane 1 was impermeable for α-lactalbumin.

used for simulations based on the mass transfer model, which has been described here above.

The clean water flux tests revealed that the Membrane 1 is significantly less permeable than M2: $2.5 \pm 1.1\,L/m^2/h/bar$ vs $58.4 \pm 9.3\,L/m^2/h/bar$ (Tijink et al., 2013) respectively, consistent with the SEM observations. The integrity of the membranes was not affected during the water permeance testing, meaning that the fabricated membranes possess sufficient mechanical strength for the dialysis and hemodiafiltration experiments.

The product of heterogeneous adsorption constant and specific surface area of activated carbon (*ak*) is refered to as a reaction kinetic parameter hereafter, for both membrane types was determined with respect to creatinine and α-lactalbumin (Table 6).

According to Table 6, the reaction kinetic parameter, ak, parameter for the adsorption of creatinine is almost twice higher for Membrane 1 than for Membrane 2. Since the membrane material and the adsorptive particles are the same for both membranes, the difference in adsorptive properties between these membranes may be attributed to the different accessibility of activated carbon particles embedded in the polymer matrix. In parallel, the comparison of adsorptive properties of Membrane 2 with respect to creatinine and α-lactalbumin demonstrates that the adsorption of the latter is significantly lower than the former (only $0.011\,s^{-1}$). This may be attributed to either a difference in steric hindrance or connected to the different affinity of activated carbon particles for creatinine and α-lactalbumin. Finally, various permeation trials with Membrane 1 revealed that it is completely impermeable for α-lactalbumin; therefore, the experimental estimation of "ak" for this case was not performed.

4.2. Double layer membrane transfer modeling

To perform the modelling of the transfer through the MMM, the boundary layer thicknesses (δ) have to be estimated. Since the validation of the model was performed with the hollow-fiber membranes placed in the module, two sets of hydrodynamic correlations, for lumen and shell sides, were used. The flow rates of feed and dialysate streams were taken from the filtration the set-up utilized during the validation experiments. The estimation of the conditions in the lumen

side was done using two following correlations (Yang et al., 2013):

$$Sh_l = 2.66Re_l^{0.25}Sc_l^{0.33}\left(\frac{d_{h_l}}{l}\right)^{0.33}; \; \delta_l = \frac{d_{h_l}}{Sh_l} \tag{16}$$

while the quantification of the hydrodynamic conditions in the shell side was done by applying another set of equations (Yang et al., 2013):

$$Sh_s = 1.25Re_s^{0.93}Sc_s^{0.33}\left(\frac{d_{h_s}}{l}\right)^{0.93}; \; d_{h_s} = \frac{\left(d_s^2 - Nd_e^2\right)}{(d_s + Nd_e)}; \; \delta_s = \frac{d_{h_s}}{Sh_s} \tag{17}$$

where d_h stands for the hydraulic diameter, N is the number of fibers, d_e and d_s are the external diameter of the membrane and of the module (shell) respectively. The selected correlations are assumed to be applicable, as they were developed for hollow fiber modules operated in laminar conditions (R < 2000), while in our experiments Re in the shell and the lumen side was below 100.

The validation experiments were conducted using feed and dialysate flow rates of 5 mL/min and 10 mL/min, respectively. Since a low concentration of solute was used for the preparation of all feed solutions and the pure phosphate buffer was used as the dialysate, the viscosity and density of both solutions were assumed to be equal to the ones of water: $10^{-3}\,Pa\,s$ and $1000\,kg/m^3$ respectively for the calculation of the boundary layer thicknesses. Based on the aforementioned hydrodynamic correlations, the thicknesses of the boundary layers in the lumen and shell sides were determined (Table 7).

The boundary layer thickness in the creatinine removal experiments differs in case of Membrane 1 and Membrane 2. This difference is ascribed to the difference in membrane dimensions (see Section 4.1). Similarly, due to the difference between the outer diameters of both membranes, the boundary layer thickness on the shell side was found smaller for Membrane 1. Similar conclusions are found for the α-lactalbumin removal experiments. The lumen boundary layers were found to be $17.9\,\mu m$ and $23.8\,\mu m$, while the shell side boundary layers are $87.1\,\mu m$ and $124\,\mu m$ for Membrane 1 and Membrane 2, respectively.

According to data presented by Shaw et al. (2009) the diffusion coefficient of creatinine in water at room temperature is $9 \times 10^{-10}\,m^2/s$, while Kim et al. (2013) used the value of $5.31 \times 10^{-10}\,m^2/s$. Therefore, here we used the average value of $7 \times 10^{-10}\,m^2/s$. To the best of our knowledge, the diffusion coefficient of α-lactalbumin was not reported in the literature. Thus with use of Einstein equation and molecule effective radius reported by Fu et al. (2005) it was calculated to be equal to $1.07 \times 10^{-10}\,m^2/s$. Finally, for the sake of simplicity we assumed that the solute diffusion coefficient is the same in the all regions of the system.

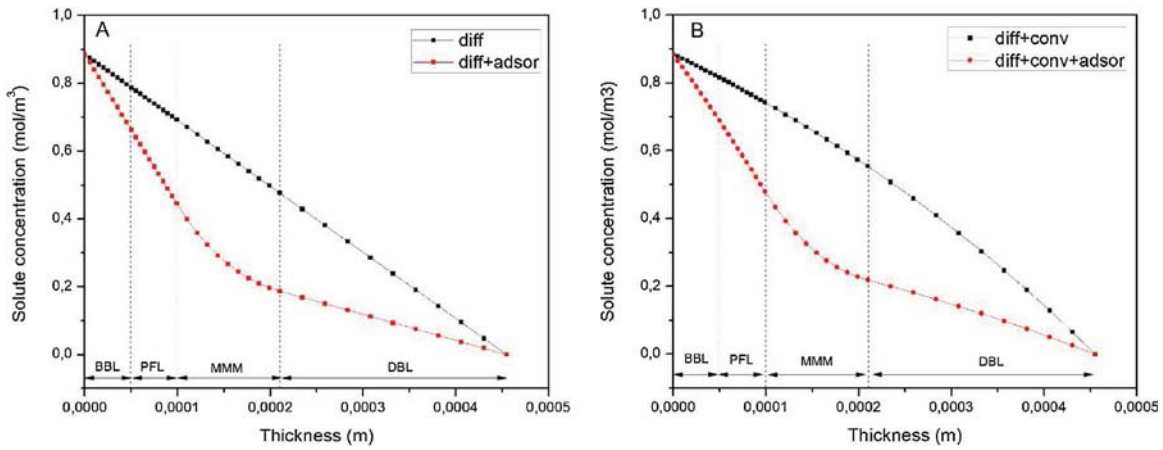| Table 7 – Boundary layer thicknesses in the validation experiments.		Membrane 1	Membrane 2
Experiment with creatinine	Lumen boundary layer, μm	30.7	45.3
	Shell side boundary layer, μm	197	245
Experiment with α-lactalbumin	Lumen boundary layer, μm	17.9	23.8
	Shell side boundary layer, μm	87.1	124

Fig. 5 – Solute concentration profiles across the membrane depending on the removal mechanisms involved. (BBL stands for blood boundary layer, PFL — particle free layer, MMM — mixed matrix membrane) (Image A — diffusion vs diffusion + adsorpsion; image B — diffusion + convection vs diffusion + convection + adsorption).

Table 8 – Input parameters applied to produce creatinine concentration profile across Membrane 2.

Name of input parameter	Value
Blood boundary layer thickness	5×10^{-5} m
Particle-free layer thickness	4.9×10^{-5} m
MMM thickness	1.11×10^{-4} m
ak parameter	$0.082\,s^{-1}$
Solute diffusion coefficient	$7 \times 10^{-10}\,m^2/s$
Thickness of dialysate boundary layer	2.3×10^{-4} m
Convective flow rate through the membrane	1.1×10^{-6} m/s[a]
Solute concentration in the blood side	$0.885\,mol/m^3$
Sieving coefficient	1

[a] Experimentally measured average convective flow rate over the filtration process.

The parameters used for our simulations have been gathered in Table 8. In principle, these parameters represent the filtration of creatinine through the Membrane 2.

The predicted solute concentration profiles across the membrane with and without adsorption have been plotted in Fig. 5, in the absence of solute in the dialysate stream.

According to Fig. 5 the presence of adsorptive particles favors the reduction of solute concentration inside the membrane. The molar flux of solute through the membrane is then more important: one can note a steeper concentration profile in the blood boundary layer (BBL). This effect is attributed to the adsorption of a fraction of the permeating species by the particles present in the MMM that is accelerating the mass transfer. Quantitative expression of such phenomena is given by the solute transfer enhancement factor (STEF) parameter provided by the model (Table 9).

From Table 9 one may conclude that for the selected set of input parameters, the addition of convective flow to solely diffusion-driven solute removal results in a 1.39 times greater
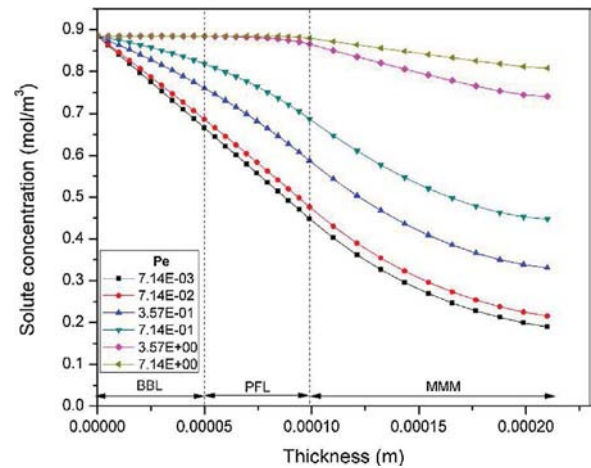

Fig. 6 – Solute concentration profile across the membrane and feed boundary layer at various rates of convective flows.

removal rate, while adsorption provides a STEF of 2.21. Moreover, the combination of all three removal mechanisms is characterized by a STEF of 2.58, meaning that compared to a pure diffusive transfer, the complete system allows to gain more than 2.5 times a flow of solute out of the feed (blood).

In parallel, the concentration inside the membrane as well as the molar flux across the membrane depend on hydrodynamics on the feed side. Fig. 6 shows the influence of convection flow rate (Peclet number) on the system, where diffusion, convection and adsorption are employed in the solute removal from the feed stream.

As it can be seen in Fig. 6, at lower values of Pe the solute concentration in the MMM is significantly different from the one in the bulk. However, at Pe > 1, when convection becomes dominant over diffusion, the solute is more effi-

Table 9 – Solute transfer acceleration for various system conditions.

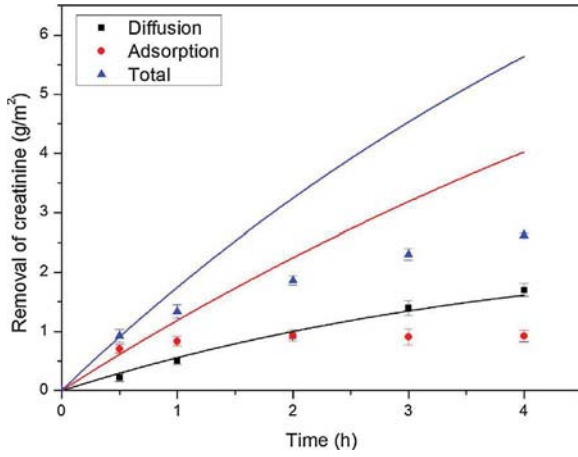| Solute removal mechanisms involved	Molar flux density, j_a	Solute transfer enhancement factor
Diffusion	$1.41 \times 10^{-6}\,mol\,m^{-2}\,s^{-1}$	1[a]
Diffusion and adsorption	$3.12 \times 10^{-6}\,mol\,m^{-2}\,s^{-1}$	2.21
Diffusion and convection	$1.95 \times 10^{-6}\,mol\,m^{-2}\,s^{-1}$	1.39
Diffusion, convection, and adsorption	$3.63 \times 10^{-6}\,mol\,m^{-2}\,s^{-1}$	2.58

[a] Taken as reference.

Fig. 7 – Results of validation experiment 1 vs theoretical prediction (continuous lines are predicted evolution of solute removal, while dots represent the experimental results).

Fig. 8 – Results of validation experiment 1 vs theoretical prediction accounting saturation of the adsorbent.

ciently transferred towards the adsorptive layer, and the bulk and membrane concentrations are close to each other. In order to keep a Pe larger than 1, the convective flow of 1.4×10^{-5} m/s or greater has to be generated. On the other hand, an excessive convection rate leads to the reduced impact of adsorption on the solute removal. Therefore, at high Pe one does not take advantage of the presence of the adsorptive capacity of the membrane.

4.3. Experimental results vs modelling

A first experiment was conducted in the diffusive mode with use of creatinine solution and Membrane 1. The experimental results are compared to the model in Fig. 7.

According to Fig. 7 the diffusive curve is ideally predicting the removal of creatinine by diffusion. Both experimental and theoretical results demonstrate that during a four-hour experiment at given conditions, one may achieve diffusive removal of 0.6 mg of creatinine in our conditions. The slight deviation of diffusive curve from linearity is a result of decrease in solute concentration in the feed and increase in the dialysate, which leads to the reduction of the driving force across the membrane. In contrary, the adsorption curve fits the experimental data only in the early stage of the process. This observation may be explained by the saturation of adsorptive particles, which suggests the presence of limiting membrane adsorption capacity. In our experiment this effect starts to be noticeable after half an hour of experiment and ultimately reaching a membrane adsorptive capacity of 0.34 mg or, more precisely, 26.27 μg of creatinine per 1 mg of membrane. Therefore, a modification of the model with the new fitted input parameter "Membrane limiting adsorption capacity" (MLAC) was done aiming to account for the activated carbon particles saturation (Fig. 8). In order to introduce this parameter in the model, the following conditions were applied:

$$\begin{cases} q < q_{max}, & r = akc \\ q \geq q_{max}, & r = 0 \end{cases} \tag{18}$$

Hence until the amount of adsorbed species (q) is inferior to the maximal capacity (q_{max}), the adsorption mechanism is active and is happening according to the previously discussed assumptions. Once the maximal membrane capacity
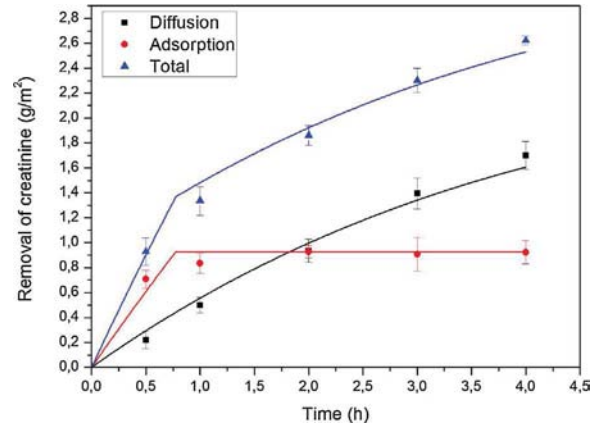
has been reached, the adsorption is no longer possible and therefore, the adsorptive removal mechanism is switched off by the model. The result of MLAC application for the experiment 1 is presented in Fig. 8.

According to Fig. 8, the removal of creatinine reaches a plateau. This could be due to saturation of particles and/or limitations in accessibility of the carbon adsorption sites by the solute under diffusive conditions. In fact, our recent work has showed that under convective conditions the adsorption and removal can significantly increase (Tijink et al., 2013)

The insertion of the limiting adsorption capacity parameter enables a rather precise prediction of the outcome of the experimental creatinine removal. Finally, the analysis showed that the adsorptive particles in the membrane enhance the transfer of creatinine by 93% within the first 45 min. Such observation provides the numerical justification of the beneficial use of dual-layer membranes with incorporated particles of activated carbon.

A validation experiment with use of creatinine solution and Membrane 1 was also conducted in hemodiafiltration mode (applying TMP). However, due to tight structure of the skin-layer in the particle free membrane the convection was limited even at high pressures, therefore the convective term had a negligible contribution to mass transfer during the experiment. Consequently, the result of this experiment was almost identical to the one with diffusive transport only (results not shown).

In addition, due to poor permeability of α-lactalbumin through Membrane 1 and its poor diffusivity through Membrane 2 during the diffusive experiment, no noticeable concentration reduction in the feed side was observed. Therefore, the results of these trials are also not presented in this paper as well.

In order to evaluate the validity of the model with respect to middle sized solutes, a second experiment was conducted with Membrane 2 and α-lactalbumin at TMP of 0.5 bar, resulting in the convective flow of 3.38×10^{-6} m/s. The results of the second experiment and their comparison with the model predictions model are shown in Fig. 9.

As shown in Fig. 9, the experimental and computed data for the diffusive+convective removal of α-lactalbumin are in very good agreement. Thanks to a significant convection rate, the removal of 2 mg of α-lactalbumin was achieved within four hours in our experimental conditions. In addition, the adsorptive removal of 0.47 mg was observed after half an hour, and did not change throughout the remaining time. This observa-
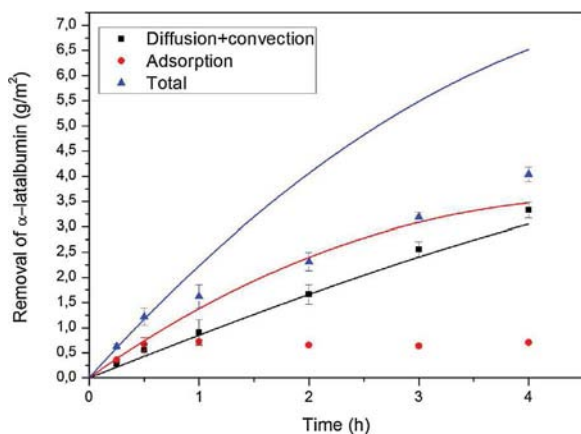
Fig. 9 – Results of validation experiment 2 vs theoretical prediction.

Fig. 10 – Results of validation experiment 2 vs theoretical prediction accounting saturation of the adsorbent.

tion indicates that, alike the first experiment, the saturation of adsorptive particles was achieved within the early stage of the process. The fast saturation may be attributed to the presence of convection, which enabled facilitated transport of protein towards the activated carbon particles. This hypothesis was supported by the analysis, which demonstrated that since convection is much faster than diffusion of α-lactalbumin, it provided 8.4 times solute transport enhancement in the beginning of the process. In the same time, the presence of the adsorptive layer resulted in 71% of protein removal facilitation. Finally, the cumulative effect of MMM and convection enabled 9.4 times greater solute removal rate at the initial moment of the experiment (t = 0) than one may expect from solely diffusion-based process given the experimental conditions used in the present research.

Since during experiment 2 the saturation of the MMM was achieved, we modified the model with the "Membrane limiting adsorption capacity" parameter as before. Based on the experimental result the input value of 8.1 μg of α-lactalbumin per mg of membrane was taken. In addition, the content of activated carbon inside Membrane 2 was previously reported to be 53% (Tijink et al., 2012). Therefore, the MLAC value may be also presented as 15.2 μg of α-lactalbumin per mg of activated carbon inside the membrane. This value is close to the experimentally measured adsorptive capacity of activated carbon powder of 15.9 μg of α-lactalbumin per mg of activated carbon.

The comparison between validation experiment 2 and modified model is shown in Fig. 10.

According to Fig. 10, the saturation of the adsorbent was reached after 30 min of experiment, and the remaining time, α-lactalbumin was removed from the feed mainly by convection and partially by diffusion.

Thus the model reveals that the MMM layer is efficient in the early stages of the process, significantly increasing the rate of removal. Beyond that point, corresponding to the saturation of the adsorbents, the rate of removal is ruled by the diffusion and convection as for a classical hemodiafiltration process.

Obtained MLAC value for Membrane 2 may be viewed from a different perspective. The module consisting of 3 fibers of 10 cm each and lumen diameter of 669 μm (Table 5) provided the total filtration area of 0.567×10^{-3} m^2, allowed an adsorptive removal of 0.47 mg of α-lactalbumin. Considering the common hemodialyser with an effective surface area of 1.5 m^2, the proportional scale-up of our module would result in 1242 mg removal of α-lactalbumin, which significantly
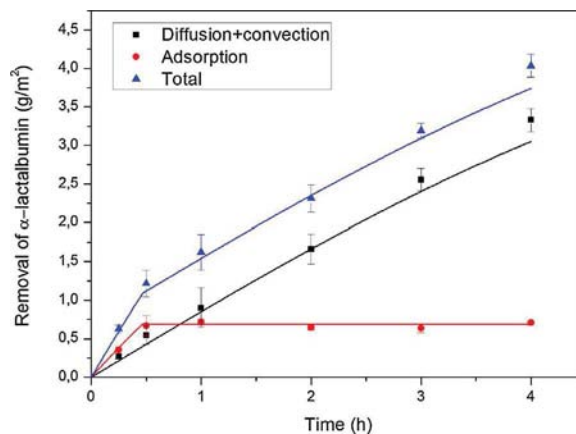
exceeds the desired β$_2$-microglobulin removal of 350–700 mg per session (based on thrice weekly treatment) (Drueke and Massy, 2009). As such, even without further optimization (reduction of lumen diameter, tuning of sieving properties, selection of proper operating conditions etc), this membrane may be effectively used for the removal middle-sized uremic toxins.

5. Conclusion

The concept of double layer membranes aiming the improvement of removal of blood toxins is a promising advancement of dialysis treatment. In the present study, we presented the model which allows more in-depth analysis of interplay of three solute removal mechanisms: diffusion, convection, and adsorption. The model demonstrated the solute concentration profile across the membrane and quantified the transfer improvement induced by the adsorption layer inside the membrane. The model was validated via comparison of model predictions with outcome of experimental testing of homemade double layer mixed matrix membranes. The developed model provides an accurate agreement with diffusive and convective removals obtained experimentally for both small and middle sized uremic toxins. Moreover, even a rather simplistic approach in the modelling of adsorptive removal of toxins (first-order reaction) provides a possibility to evaluate the amount of adsorbed species at the early stages of treatment process. The developed model may be further applied in the optimization of double layer membrane properties and the process conditions.

Acknowledgements

Appendix A.

The complete expressions for pseudo mass transfer conductances ($K_{i,j}$), which are used in Section 2.2, have the following form:

$$K_{1a} = \frac{Je^{Pe_1}}{e^{Pe_1} - 1} \tag{A.1}$$

$$K_{1b} = \frac{J}{e^{Pe_1} - 1}; \tag{A.2}$$

$$K_{2a} = \frac{Je^{Pe_2}}{e^{Pe_2} - 1}; \tag{A.3}$$

$$K_{2b} = \frac{J}{e^{Pe_2} - 1}; \tag{A.4}$$

$$K_{3a} = \frac{D_3 \sqrt{Pe_3^2 + 4\varphi^2} \cosh(\frac{\sqrt{Pe_3^2 + 4\varphi^2}}{2})}{2\delta_3 \sinh\left(\frac{\sqrt{Pe_3^2 + 4\varphi^2}}{2}\right)} + \frac{D_3 Pe_3}{2\delta_3}; \tag{A.5}$$

$$K_{3b} = \frac{D_3 e^{-\frac{Pe_3}{2}} \sqrt{Pe_3^2 + 4\varphi^2}}{2\delta_3 \sinh\left(\frac{\sqrt{Pe_3^2 + 4\varphi^2}}{2}\right)}; \tag{A.6}$$

$$K_{3c} = \frac{D_3 e^{\frac{Pe_3}{2}} \sqrt{Pe_3^2 + 4\varphi^2}}{2\delta_3 \sinh\left(\frac{\sqrt{Pe_3^2 + 4\varphi^2}}{2}\right)} \tag{A.7}$$

$$K_{3d} = \frac{D_3 \sqrt{Pe_3^2 + 4\varphi^2} \cosh(\frac{\sqrt{Pe_3^2 + 4\varphi^2}}{2}))}{2\delta_3 \sinh\left(\frac{\sqrt{Pe_3^2 + 4\varphi^2}}{2}\right)} - \frac{D_3 Pe_3}{2\delta_3} \tag{A.8}$$

$$K_{4a} = \frac{Je^{Pe_4}}{e^{Pe_4} - 1}; \tag{A.9}$$

$$K_{4b} = \frac{J}{e^{Pe_4} - 1} \tag{A.10}$$

Appendix B. Supplementary data

Supplementary data associated with this article can be found, in the online version, at http://dx.doi.org/10.1016/j.cherd.2017.08.017.

References

Barreto, F.C., Barreto, D.V., Liabeuf, S., Meert, N., Glorieux, G., Temmar, M., Choukroun, G., Vanholder, R., Massy, Z.A., 2009. Serum indoxyl sulfate is associated with vascular disease and mortality in chronic kidney disease patients. Clin. J. Am. Soc. Nephrol. 4, 1551–1558.

Busch, M., Franke, S., Ruster, C., Wolf, G., 2010. Advanced glycation end-products and the kidney. Eur. J. Clin. Invest. 40, 742–755.

Dobre, M., Meyer, T.W., Hostetter, T.H., 2013. Searching for uremic toxins. Clin. J. Am. Soc. Nephrol. 8, 322–327.

Drueke, T.B., Massy, Z.A., 2009. Beta2-microglobulin. Semin. Dial. 22, 378–380.

Eloot, S., Van Biesen, W., Vanholder, R., 2012. A sad but forgotten truth: the story of slow-moving solutes in fast hemodialysis. Semin. Dial. 25, 505–509.

Fu, B.M., Adamson, R.H., Curry, F.R., 2005. Determination of microvessel permeability and tissue diffusion coefficient of solutes by laser scanning confocal microscopy. J. Biomech. Eng. 127, 270–278.

Henrich, W.L., 2009. Principles and Practice of Dialysis, fourth ed. Lippincott Williams & Wilkins.

Kim, J.C., Cruz, D., Garzotto, F., Kaushik, M., Teixeria, C., Baldwin, M., Baldwin, I., Nalesso, F., Kim, J.H., Kang, E., Kim, H.C., Ronco, C., 2013. Effects of dialysate flow configurations in continuous renal replacement therapy on solute removal: computational modeling. Blood Purif. 35, 106–111.

Liabeuf, S., Drüeke, T.B., Massy, Z.A., 2011. Protein-bound uremic toxins: new insight from clinical studies. Toxins 3, 911–919.

Luo, F.J., Patel, K.P., Marquez, I.O., Plummer, N.S., Hostetter, T.H., Meyer, T.W., 2009. Effect of increasing dialyzer mass transfer area coefficient and dialysate flow on clearance of protein-bound solutes: a pilot crossover trial. Am. J. Kidney Dis. 53, 1042–1049.

Meyer, T.W., Peattie, J.W., Miller, J.D., Dinh, D.C., Recht, N.S., Walther, J.L., Hostetter, T.H., 2007. Increasing the clearance of protein-bound solutes by addition of a sorbent to the dialysate. J. Am. Soc. Nephrol. 18, 868–874.

Meyer, T.W., Sirich, T.L., Hostetter, T.H., 2011. Dialysis cannot be dosed. Semin. Dial. 24, 471–479.

Pavlenko, D., van Geffen, E., van Steenbergen, M.J., Glorieux, G., Vanholder, R., Gerritsen, K.G.F., Stamatialis, D., 2016. New low-flux mixed matrix membranes that offer superior removal of protein-bound toxins from human plasma. Sci. Rep. 6, 1–9.

Raj, D.S., Choudhury, D., Welbourne, T.C., Levi, M., 2000. Advanced glycation end products: a Nephrologist's perspective. Am. J. Kidney Dis. 35, 365–380.

Shaw, R.A., Rigatto, C., Reslerova, M., Ying, S.L., Man, A., Schattka, B., Battrell, C.F., Matthewson, J., Mansfield, C., 2009. Toward point-of-care diagnostic metabolic fingerprinting: quantification of plasma creatinine by infrared spectroscopy of microfluidic-preprocessed samples. Analyst 134, 1224–1231.

Tijink, M.S., Wester, M., Glorieux, G., Gerritsen, K.G., Sun, J., Swart, P.C., Borneman, Z., Wessling, M., Vanholder, R., Joles, J.A., Stamatialis, D., 2013. Mixed matrix hollow fiber membranes for removal of protein-bound toxins from human plasma. Biomaterials 34, 7819–7828.

Tijink, M.S., Wester, M., Sun, J., Saris, A., Bolhuis-Versteeg, L.A., Saiful, S., Joles, J.A., Borneman, Z., Wessling, M., Stamatialis, D.F., 2012. A novel approach for blood purification: mixed-matrix membranes combining diffusion and adsorption in one step. Acta Biomater. 8, 2279–2287.

Vanholder, R., Glorieux, G., Eloot, S., 2015. Once upon a time in dialysis: the last days of Kt/V? Kidney Int. 88, 460–465.

Walther, J.L., Bartlett, D.W., Chew, W., Robertson, C.R., Hostetter, T.H., Meyer, T.W., 2006. Downloadable computer models for renal replacement therapy. Kidney Int. 69, 1056–1063.

Yang, X., Wang, R., Fane, A.G., Tang, C.Y., Wenten, I.G., 2013. Membrane module design and dynamic shear-induced techniques to enhance liquid separation by hollow fiber modules: a review. Desalin. Water Treat. 51, 3604–3627.